

# Highly Stable Cyclic Performance of Benzoquinone-Based Organic Cathode in Aqueous Zinc Ion Batteries

Muhammad Sajid,<sup>[a]</sup> Sami Ur Rahman,<sup>[a]</sup> Fang-Yu Tao,<sup>[a]</sup> Dan Xie,<sup>[a]</sup>  
Muhammad Saif Ur Rehman,<sup>[b]</sup> Abdulwahab Salah,<sup>[c]</sup> and Jing-Ping Zhang<sup>\*[a]</sup>

An organic polymer, poly-(2,3-dithio-1,4-Benzoquinone) (PDBQ) was synthesized through condensation polymerization and characterized by SEM, EDS, XRD, FT-IR, BET, TGA, NMR and XPS. FT-IR results displayed the carbonyl and thio functionality of the material, elemental composition, and chemical states were confirmed by XPS and EDS. The material exhibited a sheet-like interconnected morphology and good thermal stability. The fabricated cathode delivered a high specific capacity of  $157.39 \text{ mAh g}^{-1}$  at a current density of  $100 \text{ mA g}^{-1}$  with high reversibility in full-cell aqueous zinc ion batteries (AZIBs). The congenital soft structure enhances the reversibility,  $\text{Zn}^{+2}$

insertion-desertion, and stability of the electrode material in coin-cell batteries. Owing to these characteristics the battery delivered higher stability with capacity retention of 97.65% after 1500 cycles and remained at 73.2% after 20,000 cycles at a high current density of  $2.0 \text{ Ag}^{-1}$  with almost 100% columbic efficiency. The energy storage behavior of the fabricated cathode was further studied by cyclic voltammetry and electrochemical impedance spectroscopy, as well as the charge storage mechanism through ex-situ FT-IR, EDS, and XPS. These results are promising to achieve the objective of stable organic material as a cathode for AZIBs.

## 1. Introduction

Lithium-ion batteries (LIBs) still dominate the energy storage market with preferred applications in electronic equipment, and electromechanical vehicles because no analogous substitute(s) is yet available.<sup>[1,2]</sup> Aqueous batteries are expected to become the most promising candidate for next-generation energy storage owing to safety, economics, and environmental benefits.<sup>[3,4]</sup> Among these, aqueous zinc ion batteries (AZIBs) have emerged as most promising due to low redox potential ( $0.76 \text{ Vs SHE}$ ), high specific capacity ( $820 \text{ mAh g}^{-1}$ ), superior kinetics and material economics.<sup>[5,6]</sup> Cathode instability, low energy density, passivation, corrosion, dendrite formation, and hydrogen evolution are some obstacles, preventing the AZIBs' commercialization.<sup>[7,8]</sup> Therefore, current research mainly focuses on designing robust materials for highly stable cathodes with enhanced energy density for AZIBs.

Transition metal sulfides/oxides, manganese (Mn) derivatives, Prussian blue analogs, and various conductive polymers have been designed to develop high-performance cathodes.<sup>[9,10]</sup> Among these, metal oxides such as  $\text{MnO}_2$ ,  $\text{V}_2\text{O}_5$ , etc., and

Prussian blue analogs have shown analogous performance.<sup>[11,12]</sup> Organic composites are selective as cathode material compared to intercalation-type inorganic counterparts due to their stable structures, rapid ionic diffusion; structural flexibility, tenability, sustainability, low density, and high surface area in addition to diverse availability and environmental friendliness.<sup>[9,13]</sup> However, the high charge impact of divalent Zn-ion ( $\text{Zn}^{+2}$ ) and its swelled hydration radius ( $\sim 4.2 \text{ \AA}$ ) are the prime impediments making most of the conventional organic structures inapt for high-performance AZIBs.<sup>[14]</sup> These apprehensions urged the development of engineered organic structures. The developed organic materials either n-type or p-type showed stable redox characteristics such as azine and carbonyl groups displayed inculcation of  $\text{Zn}^{+2}$  and/or  $\text{H}^+$  with  $=\text{N}^*$  and/or  $-\text{C}-\text{O}^*$ .<sup>[15,16]</sup> Similarly, tertiary amines and nitroxide radicals elucidate p-type redox behavior through anion delocalization with  $-\text{N}^*/-\text{HN}^*$  and  $\text{N}-\text{O}^*$ , respectively.<sup>[17,18]</sup> Conducting organic polymers (poly-aniline, polypyrrole, quinones, etc.,) exhibited similar characteristics corresponding to available functional groups.<sup>[19]</sup> Quinones/benzoquinones with intrinsic carbonyl structure could host  $\text{Zn}^{+2}$  during the charging/discharging on  $-\text{C}-\text{O}^*$ .<sup>[20,21]</sup> Quinones with para-carbonyl are superior in electrochemical performance as compared to ortho-carbonyl quinones, steric hindrance caused by ortho-positioned carbonyl restricts the  $\text{Zn}^{+2}$  ions interaction and affects the catalytic activity.<sup>[16]</sup> Therefore, Calix-4-quinone (C4Q) exhibited a high storage capacity of  $335 \text{ mAh g}^{-1}$  with a small voltage polarization of  $70 \text{ mV}$  at a current density of  $0.02 \text{ Ag}^{-1}$ .<sup>[16]</sup> The stability test showed 87% capacity retention after 1000 cycles at a current density of  $0.5 \text{ Ag}^{-1}$ . Similarly, poly(benzoquinonyl sulfide) elucidated  $203 \text{ mAh g}^{-1}$  at a current density of  $0.02 \text{ Ag}^{-1}$ .<sup>[22]</sup> A reduction of 14% in charge storage capacity was observed in only 50 cycles. Mechanism investigation proved the carbonyl group as the electrochemical active site to  $\text{Zn}^{+2}$  intercalation. Although these

[a] M. Sajid, S. Ur Rahman, F.-Y. Tao, D. Xie, J.-P. Zhang  
National & Local United Engineering Laboratory for Power Batteries, Faculty of Chemistry, Northeast Normal University, 130024 Changchun, P. R. China  
E-mail: jpzhang@nenu.edu.cn

[b] M. S. Ur Rehman  
Khwaja Fareed University of Engineering and Information Technology, Abu Dhabi Road, 54000 Rahim Yar Khan, Pakistan

[c] A. Salah  
Interdisciplinary Research Center for Hydrogen Technologies and Carbon Management, King Fahd University of Petroleum & Minerals (KFUPM), 31261 Dhahran, Saudi Arabia

 Supporting information for this article is available on the WWW under <https://doi.org/10.1002/batt.202400675>

organic materials exhibited good charge storage capacity, the reversible stability was too low to be considered for practical applications. The inherent soluble tendency, formation of soluble electrochemical intermediates, and electrochemical decay reduced the cyclic stability of organic electrodes. An inherently insoluble material, pyrene-4,4,9,10-tetraone showed relatively high cyclic stability in AZIBs.<sup>[23]</sup> Due to aqueous insolubility, the fabricated full-cell battery stabilized with 70% capacity retention at  $3\text{ Ag}^{-1}$  for 1000 cycles achieving  $145\text{ mAh g}^{-1}$  capacity. Additionally, the stability of the material is also influenced by the presence of anions in the electrolyte solution and the nature of the separator membrane. AZIBs cyclic stability increased with a proper combination of electrolyte, separator with the ability to prevent the shuttling effect, and structural modification to depress the solubility.<sup>[24,25]</sup> Structural modification through the anchoring of metals and nonmetals, oligomerization, and polymerization improved the materials' stability.<sup>[26-27]</sup> Hydrogen bonding between adjacent layers provides stiffness and improves the stability of layered organic polymers. Sun et al. illuminated the impact of intramolecular hydrogen bonding on the improved electrochemical performance of quinone polymers.<sup>[28]</sup> The synthesized 1,4-benzoquinone and 1,5-naphthalene diamine polymer showed an augmented capacity of  $137\text{ mAh g}^{-1}$  at  $25\text{ Ag}^{-1}$  in AZIBs, attributed to reduced solubility and improved charge transfer ability induced by high-density intramolecular hydrogen bonding.<sup>[28]</sup> An expanded structure, benzo[b]phenazine-6,11-dione, showed exceptionally high capacity of  $429\text{ mAh g}^{-1}$  at  $0.05\text{ Ag}^{-1}$ .<sup>[29]</sup> The fabricated cathode exhibited 73% capacity retention at  $5\text{ Ag}^{-1}$  for 10,000 cycles. This high capacity and exceptional cyclic stability are attributed to quinone and pyrazine groups existing in the material structure. These results demonstrate a high charge storage capacity of organic materials with carbonyl groups. However, the applicability of organic materials is deprived of inferior stability in AZIBs. Structure modification and intramolecular H-bonding could solve instability concerns resulting in improved stability and electrochemical performance.

Inspired by this outcome, a straight-chain polymer, poly-(2,3-dithio-1,4-Benzoquinone) (PDBQ) was synthesized by the sulfidation of tetrafluoro-1,4-benzoquinone followed by polymerization with activated tetrachloro-1,4-benzoquinone (Scheme S1). The synthesized co-polymer maintains dual functionality owing to quinone and thio-linkage as shown in scheme S2. Repeated benzoquinone units hold a well-established localized enolization mechanism which is highly reversible and increases the stability of developed structures.<sup>[16,30,31]</sup>

Two thio-linkages develop a new hetero-ring with S at 1 and 4 (O & O') positions. This hetero-cycle could oxidize losing two electrons ( $e^-$ ) through anionic delocalization, thus improving the charge storage capacity.<sup>[32]</sup> Consequently, the developed layered network of alternative benzoquinone and thio linkage possesses four potentially available sites for  $\text{Zn}^{+2}$  insertion/desertion. Hence, the synthesized structure expounded high charge storage capacity and remarkably high stability in AZIBs.

## Experimental Section

### Polymer Synthesis

Tetrafluoro-1,4-benzoquinone (TFBQ,  $\text{C}_6\text{F}_4\text{O}_2$ ), Tetrachloro-1,4-benzoquinone (TCBQ,  $\text{C}_6\text{Cl}_4\text{O}_2$ ), Sodium sulfide ( $\text{Na}_2\text{S}$ ), N, N-Dimethyl formamide (DMF), Ethanol ( $\text{C}_2\text{H}_5\text{OH}$ ), Zinc perchlorate hexahydrate ( $\text{Zn}(\text{ClO}_4)_2 \cdot 6\text{H}_2\text{O}$ ) and Hydrochloric acid (HCl) were procured from aladdin scientific. Analytical grade ingredients were acquired and used without any further purification. Ultra-pure water was obtained from the system available in the lab.

An organic co-polymer (PDBQ) was synthesized following the procedure already reported in the literature with slight modifications according to the method illustrated in Figure 1a and Scheme S1.<sup>[33-35]</sup> Briefly, 8 mmol of TFBQ was mixed with 30 mmol of sodium sulfide in a 50% ethanol solution and continuously stirred for 3 hours maintaining the solution temperature at  $\sim 80^\circ\text{C}$  (solution I). A similar quantity of TCBQ was thoroughly homogenized in a round bottom flask by stirring for 10 minutes in a 50 mL DMF solution (solution II). Solution II is then transferred to solution I gently with continuous stirring. The reaction mixture refluxed for 12 hours followed by cooling to room temperature. The material was collected through filtration via a 0.8-micron filter assembly after adjusting the solution  $\text{pH}=3.5 \pm 0.4$ , washed and dried at  $60^\circ\text{C}$  overnight under vacuum, and preserved.

### Material Characterization

The prepared PDBQ was characterized using X-ray powder diffraction (XRD, Smartlab radiation), Fourier-transformed infrared spectroscopy (FT-IR) and solid-state  $^{13}\text{C}$  nuclear magnetic resonance (NMR). Oxidation states were examined through X-ray photo-electron spectroscopy (XPS). The microstructures were examined using a field emission scanning electron microscope (SEM, SU8000). Thermal stability was analyzed by Thermogravimetric analysis (TGA, PerkinElmer Thermal Analysis) up to  $800^\circ\text{C}$  with an increment of  $10^\circ\text{C min}^{-1}$ . The specific surface area and pore size distribution were analyzed through Nitrogen ( $\text{N}_2$ ) adsorption-desorption isotherms on the BET instrument (Quantachrome) at  $77.35\text{ K}$  and the molecular weight through size exclusion chromatography (SEC) using refractive index (RI) detector.

### Battery Fabrication and Electrochemical Measurement

The electrodes were prepared using synthesized polymer (65%), conductor (super P, 25%), and polyvinylidene fluoride (PVDF, 10%) as the binder. The dry mixture was mixed meticulously in a mortar followed by regimented mixing using N-Methyl-2-Pyrrolidone (NMP) solvent. The homogenized slurry was distributed uniformly over a substrate (Ti, etc.) and dried overnight at  $60^\circ\text{C}$  under vacuum. The mass loading was 1.0 to  $1.3\text{ mg cm}^{-2}$  (after drying). The microscopic images of freshly prepared and used electrodes are provided in Figure S1.

Coin cell full batteries (CR2032) were assembled employing zinc anode and prepared electrode as the cathode in setting Whatman glass fiber (pore size =  $2.7\text{ }\mu\text{m}$ , and  $\Phi=16\text{ mm}$ ) as the permeable membrane.  $100\text{ }\mu\text{L}$  of 3.5 molar aqueous solution of zinc perchlorate was used as the electrolyte. Electrochemical impedance spectroscopy (EIS) measurements were performed between 0.01 Hz to 100 kHz at various amplitudes in the potential range of 0.2 to 1.6 V. A CHI660E electrochemical work station was used to measure the EIS and Cyclic voltammetry (CV). Galvanostatic charge-discharge (GCD) experiments were performed over the Neware battery testing system applying 0.2–1.6 V (vs.  $\text{Zn}^{+2}/\text{Zn}$ ) at room temperature.

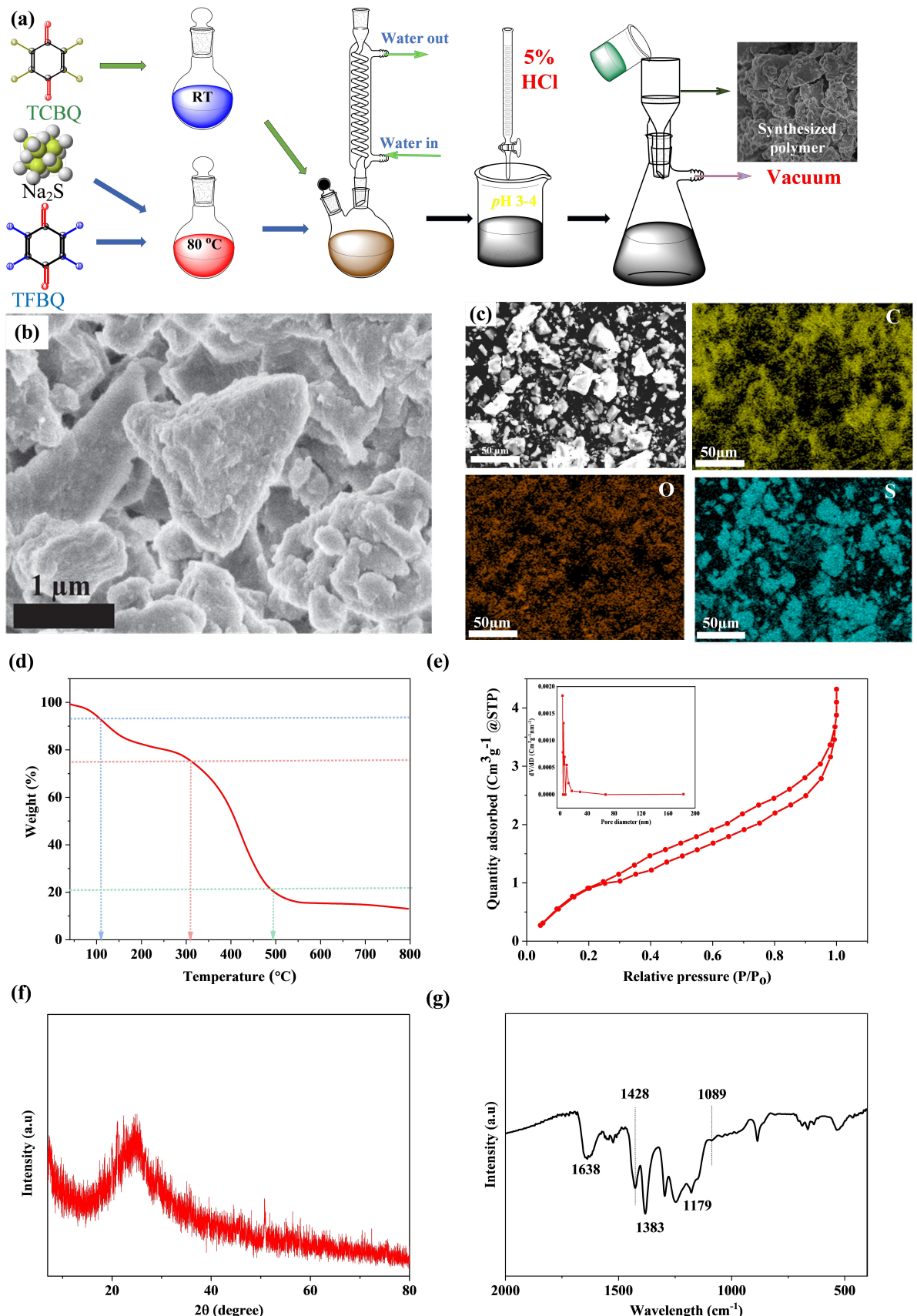


**Figure 1.** (a) Synthesis scheme for PDBQ from TFBQ and TCBQ copolymerization, (b) SEM, (c) EDS mapping, (d) TGA, (e) N<sub>2</sub> adsorption-desorption curve and pore size distribution (inset) of as-synthesized polymer, (f) XRD, and (g) FT-IR.

## 2. Results and Discussion

### 2.1. Structural and Morphological Characterization

Figure 1b, the SEM micrograph of the synthesized PDBQ shows a sheet-like well-interconnected structure free from agglomeration, demonstrating an improved surface morphology.<sup>[36]</sup> The EDS mapping (Figure 1c) professes the uniform distribution of basic elements, C, O, and S in the material cluster signifying the successful synthesis of the material. Figure 1d illustrates the thermogram of as-synthesized material which shows three-step weight loss. The first weight loss occurred in the temperature range of 30–104.9 °C which is characteristically ascribed to the moisture contents of the sample. The second weight loss occurred between 105–305 °C, attributed to the unreacted organic contents in the polymer matrix.<sup>[28]</sup> The third and last weight loss occurred between 305–487 °C, typically a backbone degradation of the synthesized polymer. Thus, thermal stability up to 487 °C is well aligned with its utilization as the electrode material in AZIBs. The N<sub>2</sub> adsorption-desorption curve as shown in Figure 1e, is typically a type IV adsorption curve with a hysteresis loop (the inset is a pore size distribution curve).<sup>[37]</sup> From the BET data, the calculated pore volume and specific surface area are 0.011 cm<sup>2</sup> g<sup>-1</sup> and 41.67 m<sup>2</sup> g<sup>-1</sup> respectively. Figure 1f, XRD spectrum of synthesized PDBQ, shows a well-defined single peak at 24.9°, demonstrating the porous amorphous structure of the polymer.<sup>[33]</sup> The XRD results correlate with SEM and BET analyses.

Figure 1g depicts the FT-IR spectrum of the PDBQ polymer. The absorption band at 1638 cm<sup>-1</sup> indicates the structural vibration of the carbonyl group.<sup>[29,33,38]</sup> The well-defined peaks at 1428 cm<sup>-1</sup>, 1383 cm<sup>-1</sup>, 1179 cm<sup>-1</sup>, and 1089 cm<sup>-1</sup> indicate C–S linkage.<sup>[35,39]</sup> Hence, these peaks reveal the successful incorporation of thio linkages (–C–S–C–) and carbonyl ( $\text{C}=\text{O}$ ) groups in the polymer chain. Figure S2 displays the <sup>13</sup>C solid state NMR spectrum of the synthesized PDBQ. Two distinct peaks appeared at 140.7 and 160.8 ppm, which are associated with C–S and C=O, respectively. No other C signals are detected, which confirms the successful synthesis of the polymer. The lower shift in carbonyl peak advocates the conjugation of  $\pi$ -electrons on polymerization that stabilized the carbonyl through resonance.<sup>[40–42]</sup> Further, the molecular weight of the synthesized polymer was determined using SEC (Figure S3a, b). The average molecular weight (Mw) of PDBQ was 30402 as illustrated in Figure S2a, favorable for high delocalization of  $\pi$ -electron.<sup>[33]</sup> Furthermore, the calculated degree of polymerization and polydispersity from SEC data are 176 and 1.85, respectively. These results manifested the high stability and dispersity of the material, promising for energy storage applications.

XPS was performed to determine the composition and oxidation states of the synthesized PDBQ. XPS survey spectrum (Figure 2a) signifies Sulfur (S), Carbon (C), and Oxygen (O) as the principal constituents of the polymer in the range of 0–1000 eV. Typically, the distinct peaks at 164.25 eV, 284.75 eV, and 532.4 eV, correspond to S, C, and O respectively (Fig-

ure 2a).<sup>[36,43,44]</sup> Figure 2b shows the high-resolution C 1s spectrum with three centered peaks at 284.89 eV, 286.39 eV, and 288.1 eV matching C–C/C=C, C–S, and C=O, respectively.<sup>[43,45–48]</sup> Figure 2c, high-resolution S 2p spectrum shows two strong peaks at 164.25 eV and 165.45 eV, revealing the existence of two states of S as S 2p<sub>3/2</sub> and S 2p<sub>1/2</sub>, respectively in the polymer structure.<sup>[36,43]</sup> Figure 2d, O 1s spectrum, shows two distinct peaks for C=O and C–O at 532.4 eV and 533.7 eV, respectively.<sup>[37,49]</sup> The peak intensity for C–O is low as compared to C=O suggesting a higher concentration of C=O in the polymer structure revealing the existence of a high  $\pi$  conjugation, consequently producing delocalized electrons in the polymer structure.

### 2.2. Electrochemical Performance

All the electrochemical analyses were performed in assembled coin cell batteries using PDBQ and Zn metal as cathodes and anodes, respectively. The supporting information, Figures S4–S6, displays the electrochemical performance of the PDBQ material at different substrates using different electrolyte solutions and different concentrations of Zn(ClO<sub>4</sub>)<sub>2</sub>. The results clearly identified Ti as the most promising substrate and 3.5 M Zn(ClO<sub>4</sub>)<sub>2</sub> as the optimal electrolyte solution, which was then maintained in all subsequent electrochemical experiments.

The electrochemical behavior of the fabricated coin cell battery was retrieved through CV between 0.2–1.8 V; subsequent CV curves are shown in Figure 3a. The illustrated CV curves have two distinct oxidation and one reduction peak, demonstrating the redox process in the PDBQ cathode. Lighter peak variation in the successive curves after the very first peak is probably due to the formation of a solid electrolyte interface (SEI) layer.<sup>[50,51]</sup> After the initial three cycles, the CV cycles overlap indicating the superior reversible stability and fast reaction kinetics of the cathode material. EIS measurements were performed to investigate the series resistance ( $R_s$ ) and charge transfer resistance ( $R_{CT}$ ). The corresponding Nyquist plots of freshly prepared battery are shown in Figure 3b and after various GCD cycling in Figure S7. The Nyquist plot can be divided into three main regions. The high-frequency region near the real axis represents  $R_s$ , the solution resistance between the electrolyte and electrode interphases on both ends of the membrane separator. The semicircle region (region II) in the medium frequency represents  $R_{CT}$ , charge transfer resistance on the electrode and electrolyte interfaces as well as inside the bulk of electrode material.<sup>[52]</sup> The inclined line (region III) in the low-frequency region represents the diffusion limitation of the electrolyte. EIS analysis shows 1.52 and 105.39 Ω·cm<sup>2</sup> as the  $R_s$  and  $R_{CT}$ , respectively. These low  $R_s$  and  $R_{CT}$  values can be attributed to the well-interconnected porous structure of the polymeric material and validate the quality of the developed structure as an impactful electrode material with low resistances, hence promising for electrochemical applications. Further EIS was performed after 100, 200, and 500 GCD cycles at 0.1 Ag<sup>-1</sup> and the obtained Nyquist plots have been displayed in Figure S7, and the corresponding  $R_s$  and  $R_{CT}$  values are

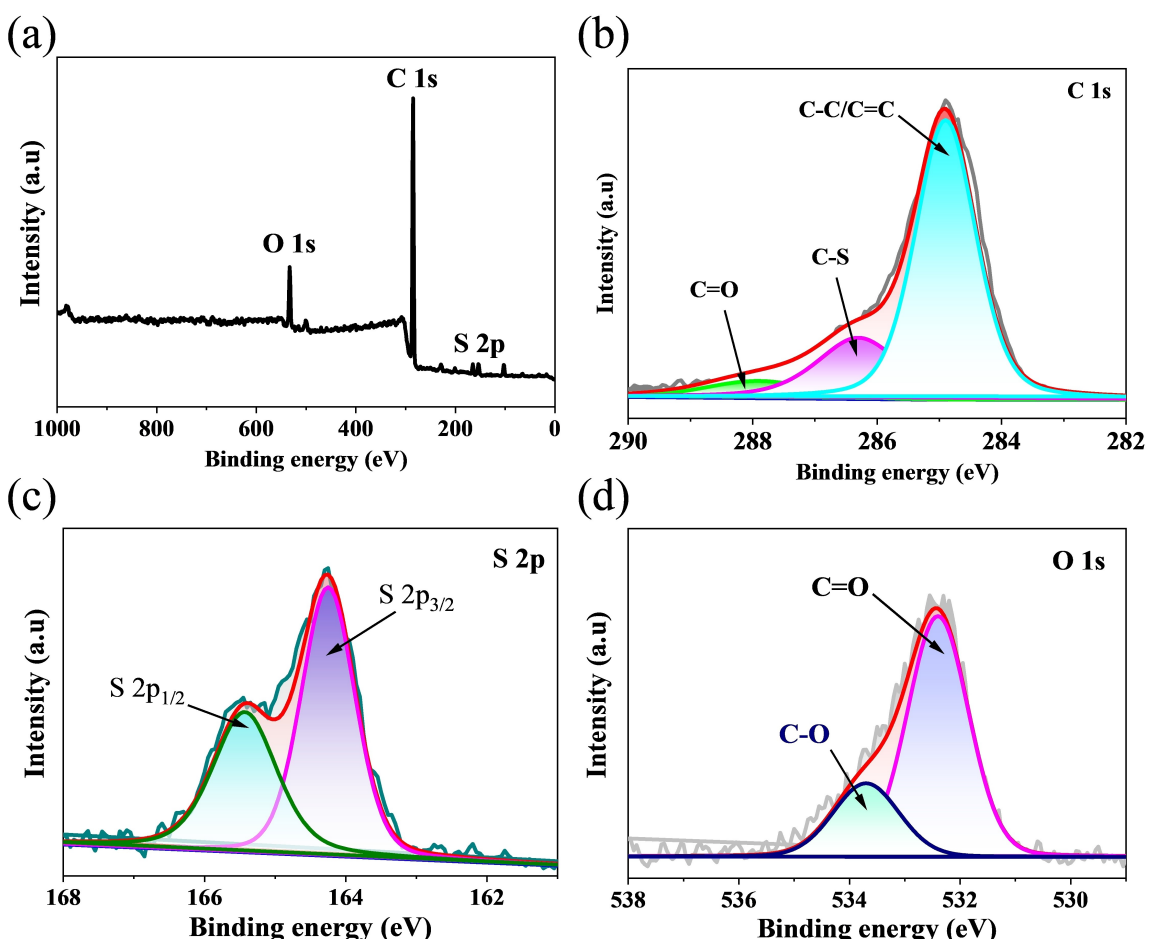


Figure 2. XPS spectrum of PDBQ (a) and spectrum of (b) C 1s, (c) S 2p, and (d) O 1s.

tabulated in Table S1. The  $R_s$  and  $R_{CT}$  values show no significant variation. These results manifested a good structural stability and charge transfer ability of the material, which is critical to achieving the higher stability of charge storage devices.

The assembled coin cell battery underwent galvanostatic charge-discharge at various current densities. Before optimization, the freshly prepared batteries showed low initial capacity and achieved stable discharge capacity after a few cycles. As shown in Figure S8, the initial discharge capacity was 39.78 mAh g<sup>-1</sup>, and it achieved a stable discharge capacity of 151.13 mAh g<sup>-1</sup> for the 48<sup>th</sup> cycle. For the initial few cycles, the low discharge capacity is obvious due to the limited diffusion of electrolytes in the bulk of cathode material, a common observation of AZIBs.<sup>[53,54]</sup> Afterward, the assembled batteries were applied for GCD measurement after providing eight hours of stabilizing time for each battery. Figure 3c displays the conditional GCD curves from cycles 1 to 100. The fabricated battery with PDBQ cathode elucidated an initial discharge capacity of 157.39 mAh g<sup>-1</sup> for the first cycle and retained 149.6 mAh g<sup>-1</sup> after 100 cycles. This minor decrease in charge storage capacity is partially due to the establishment of SEI film.<sup>[55]</sup> Figure 3d displays the cyclic stability of the battery for 100 cycles at 0.1 Ag<sup>-1</sup> having a capacity retention of 95.05 %. This small capacity fading proves the stability of the fabricated

cathode in full cell AZIBs. Hence, the fabricated battery was applied for GCD measurement at different current densities. Figure 4a displays GCD curves at different current densities. As illustrated, the battery delivered 153.06, 135.94, 119.34, 109.39, 92.87, 84.5, and 73.8 mAh g<sup>-1</sup> discharge capacity at 0.1, 0.2, 0.3, 0.5, 1.0, 1.5, and 2.0 Ag<sup>-1</sup>, respectively. Figure 4b illustrates the rate performance of the battery for five cycles at each current density applied. Figure 4b shows that the battery nearly regained its initial capacity during reverse cycling at 0.1 Ag<sup>-1</sup>.

The contribution of conductive additive (super P) was evaluated by applying a cathode with 90% super P and 10% PVDF (without PDBQ). The contribution of conductive additive was only 0.19 mAh g<sup>-1</sup> (Figure S9), negligible to the total capacity of the battery. The long-term cycling stability, measured at a higher current density of 2.0 Ag<sup>-1</sup> is displayed in Figures 4d and 4e. As illustrated in Figure 4d, initially the discharge capacity remained stable till 1590 cycles with 97.65 % capacity retention and then declined. After 10,000 cycles the discharge capacity was 55 mAh g<sup>-1</sup> showing an overall capacity retention of 74.34 % of the initial discharge capacity value i.e. 73.24 mAh g<sup>-1</sup>. The recorded overall capacity decay was 25.6 % and the capacity fading rate was 0.0018 mAh g<sup>-1</sup> per cycle. It is worth mentioning that the voltage profile was still well sustained with the observation of a single typical plateau during

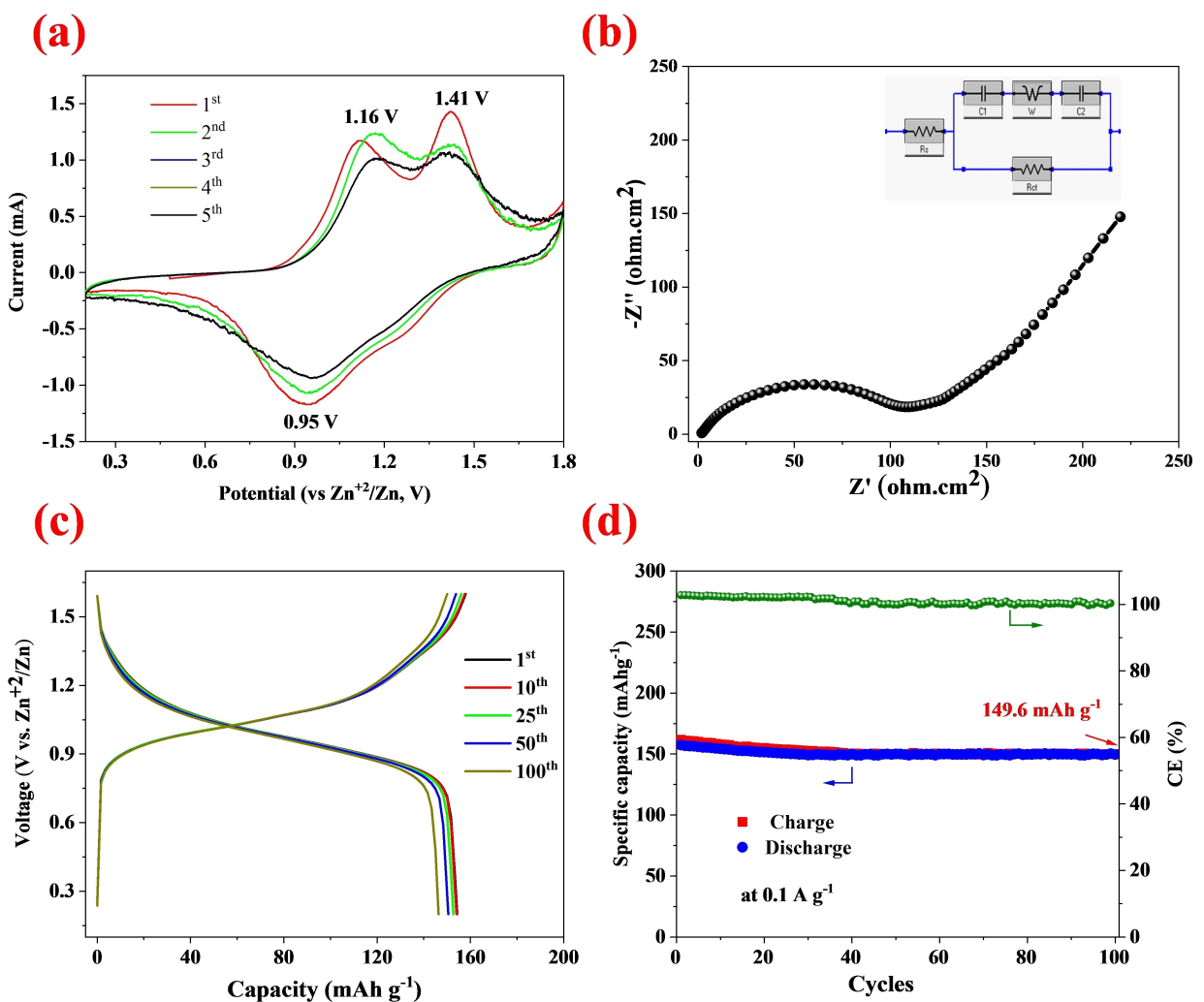


**Figure 3.** Electrochemical performance of coin cell AZIBs with PDBQ cathode (a) CV curves at  $3 \text{ mVs}^{-1}$ , (b) EIS, (c) GCD curves, and (d) cyclic stability at a current density of  $0.1 \text{ Ag}^{-1}$ .

the GCD process (Figure S10a). The same battery was again subjected to GCD cycling at  $2.0 \text{ Ag}^{-1}$  after resting for 72 hours. As depicted in Figure 4e, the battery showed exceptionally higher stability in the second spell of 10,000 GCD cycles with a capacity retention of 97.5%. The capacity fading was extremely low i.e.  $1.38 \times 10^{-4} \text{ mAh g}^{-1}$  per cycle. The single typical charge/discharge plateau, Figure S10b, again inveterate the outstanding stability of the cathode even after 20,000 GCD cycles. Collectively, these results signify the outstandingly augmented reversible cyclic stability of PDBQ in AZIBs, vital for the commercial development of organic AZIBs. The obtained results are compared with quinone-based cathode AZIBs as shown in Figure 4c and Table S2. Comparative results illuminate the PDBQ selectivity due to its stupendously high stability, 73.2% discharge capacity retention after 20,000 cycles (Table S2). The obtained results can be considered to remove the instability concerns of organic cathodes in AZIBs.

To explore the charge storage mechanism, a full-cell battery was assembled and applied for CV testing at various scan rates between 0.2 and 1.6 V. As evident from Figure 5a, the redox

peaks expanded holding a similar trend with scan rate increase elucidating the rapid charge transfer process and amplified electrochemical kinetics. The trend was quite similar even at a high scan rate of  $3 \text{ mVs}^{-1}$ , validating the stability of the PDBQ cathode at a higher scan rate.

The dependency of peak current ( $I_p$ ) on scan rate ( $v$ ) of CV is described as (eq. i & ii)

$$I_p = av^b \quad (\text{i})$$

$$\log(I_p) = \log(a) + b \log(v) \quad (\text{ii})$$

where  $a$  and  $b$  are variables illuminating the behavior of electrochemical reactions. In any real electrochemical process,  $b$  is always between 0.5 and 1; if  $b$  approaches 0.5, it represents a diffusion-controlled process, and  $b$  approaching 1 shows a pseudocapacitive process.<sup>[56]</sup> The calculated  $b$  values for redox peaks of CV curves (Figure 5a) are 0.79, 0.84, and 0.78 as depicted in Figure 5b, signifying the synergistic effect of

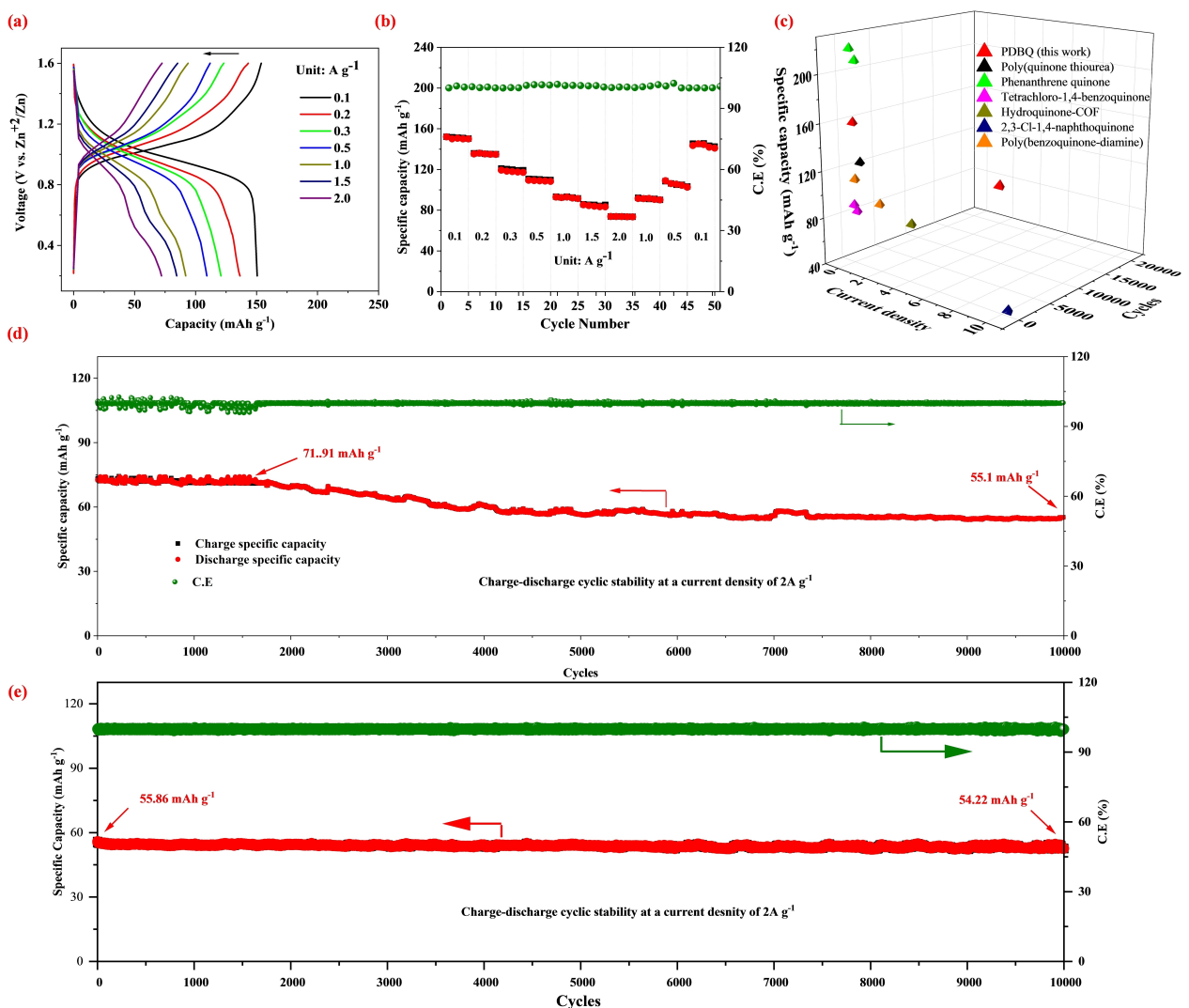


**Figure 4.** Electrochemical performance of synthesized PDBQ as a potential cathode in AZIBs (a) GCD curves at different current densities, (b) rate performance at different current densities, (c) comparison of electrochemical performance between different quinone-based materials, and (d, e) Elongated cycling stability at a current density of 2 A g<sup>-1</sup>.

diffusion and capacitive behavior. The contribution of each capacitance can be calculated through eq. iii;<sup>[57]</sup>

$$I_p = k_1 v + k_2 v^{0.5} \quad (\text{iii})$$

$$\frac{I_p}{v^{0.5}} = k_1 v^{0.5} + k_2 \quad (\text{iv})$$

where,  $k_1 v$  and  $k_2 v^{0.5}$  in eq. iii represents the share of pseudocapacitive and diffusion-control, respectively.<sup>[58]</sup> Eq iv is the derived form and the graph between  $\frac{I_p}{v^{0.5}}$  and  $v^{0.5}$  gives the straight line with  $k_1$  slope and  $k_2$  as the y-intercept. The electrochemical contribution calculated by this graphical method (Figure S11), shows the capacitive contribution of 19.27, 41.59, 53.15, and 67.41 for 0.2, 0.5, 2.0, and 3.0 mVs<sup>-1</sup>, respectively (Figures 5c and 5d). The gradual increase in capacitive contribution with an increase in scan rate is ascribed to the limited access of the electrolyte into the cathode

material.<sup>[40]</sup> In addition, the high scan rate reduced the time for interlayer diffusion resulting in reduced diffusive control and improved capacitive contribution.

The charge storage mechanism and redox kinetics were explored through ex-situ FT-IR, EDS, and XPS analyses. Figure 6a shows the charge/discharge points at which the electrochemical reaction ceased and recorded FT-IR spectra at these points are displayed in Figure 6b. The shifting of functional groups and peak intensity variation shows the electrochemical reaction pathway in organic structures.<sup>[33,59]</sup> It can be observed from FT-IR spectra that the carbonyl group texted at 1656 cm<sup>-1</sup> remains constant from point a→c showing disengagement of the carbonyl group during initial charge. However, the intensity of C–S peaks (1422, 1381, and 1243 cm<sup>-1</sup>) gradually reduced indicating the C–S involvement.<sup>[59]</sup> During the discharge process from 1.6 to 0.2 V, the intensity of the carbonyl peak reduced from point c→f, while during the charging process from 0.2 to 1.6 V (f→i), its intensity gradually increased, revealing the

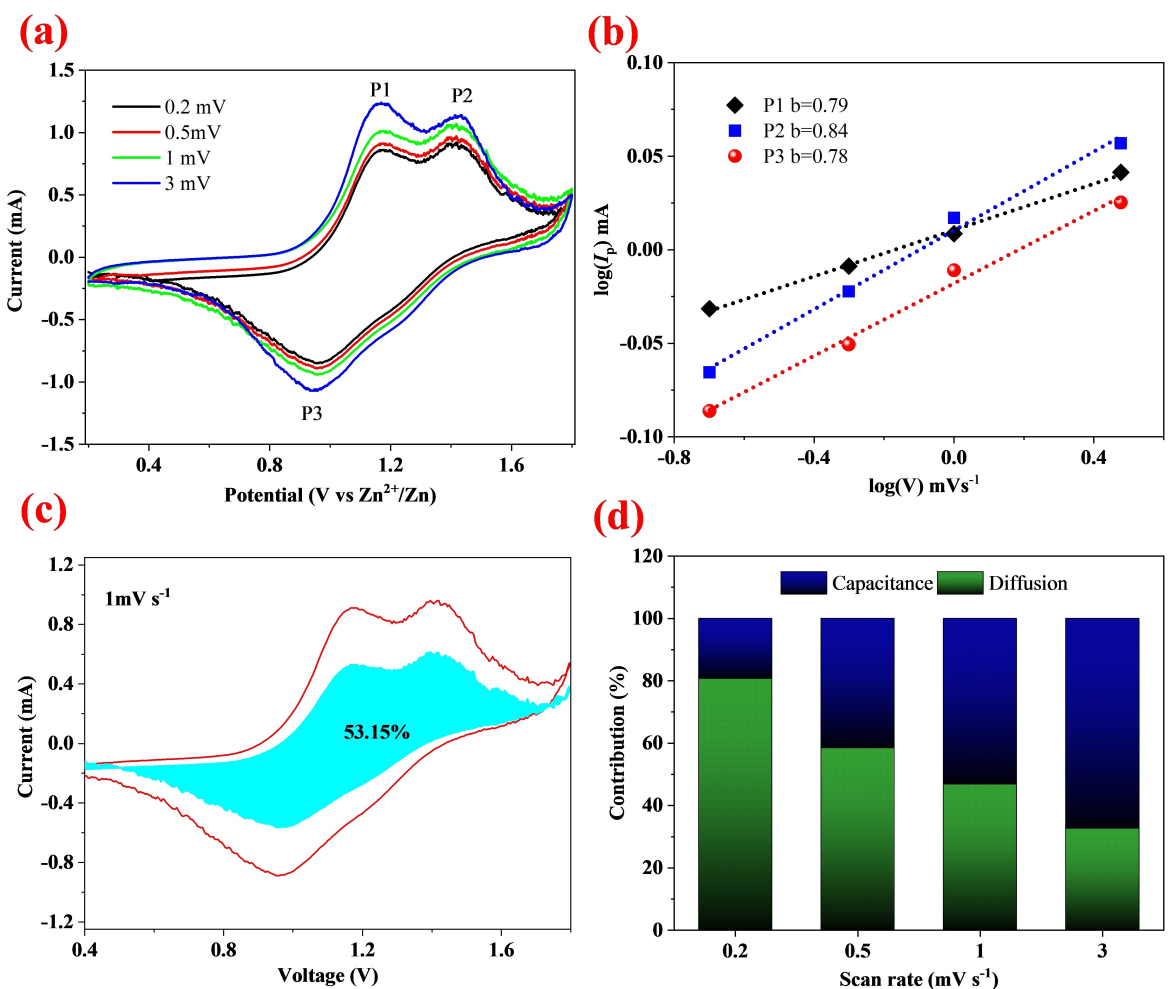


**Figure 5.** (a) CV curves at different scan rates, (b) linear fitting of  $\log(I_p)$  vs  $\log(v)$  derived from CVs, (c) CV at 1 mV s<sup>-1</sup> showing capacitive contribution as a shaded area, (d) ratios of diffusion (green) and pseudocapacitive (blue) contributions for full cell AZIBs.

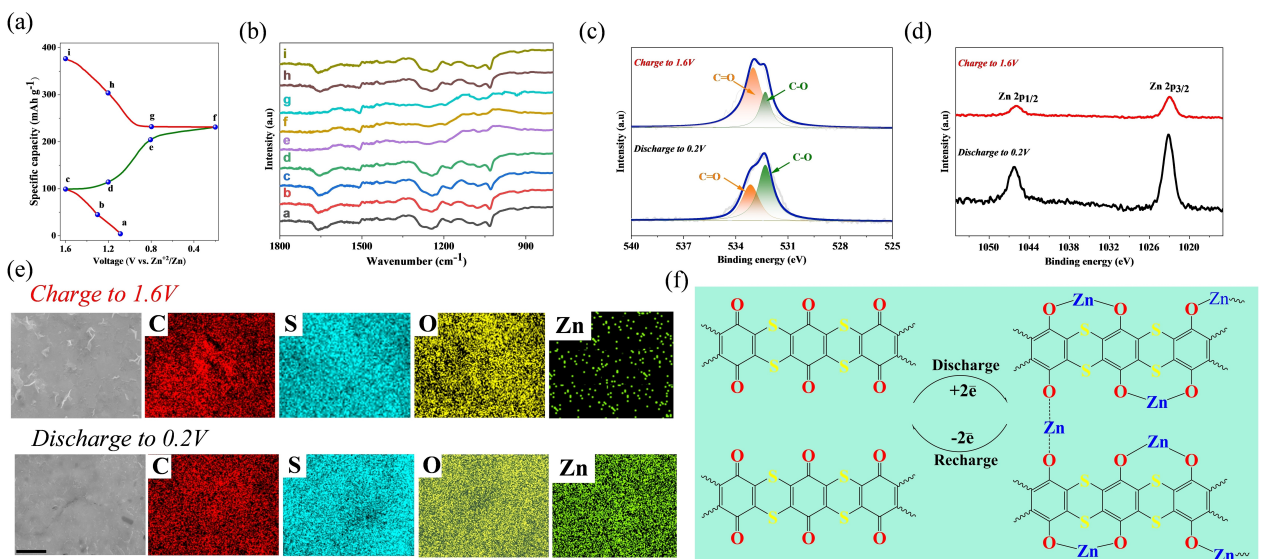


**Figure 6.** Kinetic evaluation (a, b) ex-situ FT-IR, XPS spectra at charged and discharged state for (c) O 1s and (d) Zn 2p, (e) EDS mapping of electrodes at charged and discharged state with 10  $\mu$ m scale bar and (f) plausible redox mechanism.

involvement of C=O in the redox process of PDBQ cathode (Figure 6b). Carbonyl peak intensity is very low at points e, f, and g, suggesting complete involvement in the redox process of the cathode. XPS spectra, Figure 6c, confirm this pathway showing variation in C=O and C–O intensities at charge/discharge states in the O 1s spectrum. A comparative reduction in Zn 2p intensity on charging from 0.2 to 1.6 V (point f→i) proves the reversible insertion of Zn<sup>+2</sup> into the structure of the PDBQ cathode (Figure 6d).<sup>[33]</sup> EDS elemental mapping further confirms the reversible intake of Zn<sup>+2</sup>. Figure 6e illustrates a high intensity of Zn contents at the discharge state (point f) compared to the charge state (point i) in the PDBQ cathode. EDS results are consistent with FT-IR and XPS findings, proving reversible sorption of Zn at the carbonyl site during the redox process.<sup>[33,60]</sup> Based on these observations, the plausible mechanism presented in Figure 6f shows the Zn<sup>+2</sup> insertion at adjacent carbonyls, gaining two electrons (2e<sup>-</sup>) in a discharge process.<sup>[59]</sup> In addition, some Zn<sup>+2</sup> might be stored through inter-layer coordination as shown in Figure S12.<sup>[61]</sup> Hence, considering these results, the formation of C–O–Zn–O–C can be safely illustrated as a preferred charge storage site.<sup>[33,61]</sup>

All these results suggest that the synthesized PDBQ polymer is a good electrode material for AZIBs. Its ultra-high stability and flexible structure make it a highly suitable material for soft-packing batteries and other energy storage devices.

### 3. Conclusions

A conjugated polymer, PDBQ was synthesized from tetrafluoro-1,4-benzoquinone and tetrachloro-1,4-benzoquinone by condensation polymerization. The synthesized PDBQ polymer as a cathode exhibited remarkable electrochemical stability in aqueous zinc ion batteries, owing to the high density of π-π interaction in the structure. The assembled coin cell battery delivered a high-capacity retention of 73.2% (20,000 cycles in two spells at 2 Ag<sup>-1</sup>), promising to eradicate the stability concern from organic AZIBs. The structural investigation revealed carbonyl oxygen as the preferred Zn<sup>+2</sup> insertion/desertion site. This exceptionally high stability and inherited soft structure could satisfy the requirements of safe and flexible batteries for portable gadgets and other energy storage applications.

### Author Contributions

**Muhammad Sajid:** Conceptualization, Investigation, Methodology, Data curation, Writing-original draft, **Sami Ur Rahman:** Formal analysis, Software, Writing-review & editing, **Fang-Yu Tao:** Resources, Methodology, **Dan Xie:** Visualization, Validation, **Muhammad Saif Ur Rehman:** Writing-review & editing, Validation, **Abdulwahab Salah:** Software, Methodology, **Jing-Ping Zhang:** Funding acquisition, Supervision.

### Acknowledgements

This work was supported by the Postdoctoral Fellowship Program of CPSF (GZC20230409), the National Natural Science Foundation of China (21873018, 21573036), and the open project of the Jilin Province Key Laboratory of Organic Functional Molecular Design & Synthesis (130028655) are greatly acknowledged.

### Conflict of Interests

The authors declare there are no known competing interests to declare.

### Data Availability Statement

Data will be made available on request.

**Keywords:** Aqueous zinc ion batteries · conducting polymers · organic cathode · high stability

- [1] Y. Zhang, Y. Li, S. Yao, N. Ali, X. Kong, J. Wang, *Energy Storage Mater.* **2024**, *71*, 103544.
- [2] L. Wang, N. Liu, X. Zhao, X. Wang, T. Zhang, Z. Luo, F. Li, *Chem. Sci.* **2024**, *15*, 2133.
- [3] G. Li, L. Sun, S. Zhang, C. Zhang, H. Jin, K. Davey, G. Liang, S. Liu, J. Mao, Z. Guo, *Adv. Funct. Mater.* **2024**, *34*, 2301291.
- [4] Y. Li, J. Wang, Z. Tian, F. Lai, T. Liu, G. He, *Batteries & Supercaps* **2023**, *6*, e202200509.
- [5] Y. Zhao, Y. Huang, F. Wu, R. Chen, L. Li, Y. Zhao, Y. Huang, F. Wu, R. Chen, L. Li, *Adv. Mater.* **2021**, *33*, 2106469.
- [6] P. Yu, Y. Zeng, H. Zhang, M. Yu, Y. Tong, X. Lu, *Small* **2019**, *15*, 1804760.
- [7] Q. Zhang, P. Zhi, J. Zhang, S. Duan, X. Yao, S. Liu, Z. Sun, S. C. Jun, N. Zhao, L. Dai, L. Wang, X. Wu, Z. He, Q. Zhang, *Energy Storage Mater.* **2024**, *73*, 103797.
- [8] M. Ma, M. Du, Y. Liu, H. Lü, J. Yang, Z. Hao, J. Guo, X. Wu, *Particuology* **2024**, *86*, 160.
- [9] G. Zampardi, F. La Mantia, *Nat. Commun.* **2022**, *13*, 687.
- [10] D. Xie, Y. Sang, D. H. Wang, W. Y. Diao, F. Y. Tao, C. Liu, J. W. Wang, H. Z. Sun, J. P. Zhang, X. L. Wu, *Angew. Chem. Int. Ed.* **2023**, *62*, e202216934.
- [11] H. Li, S. Guo, H. Zhou, *Energy Storage Mater.* **2023**, *56*, 227.
- [12] Z. Song, L. Miao, L. Ruhmann, Y. Lv, L. Li, L. Gan, M. Liu, *Angew. Chem.* **2023**, *135*, e202219136.
- [13] H. Cui, T. Wang, Z. Huang, G. Liang, Z. Chen, A. Chen, D. Wang, Q. Yang, H. Hong, J. Fan, C. Zhi, *Angew. Chem. Int. Ed.* **2022**, *61*, e202203453.
- [14] Y. Xiao, J. Ren, M. Li, K. Xiao, Y. Wang, *Chem. Eng. J.* **2023**, *474*, 145801.
- [15] Z. Tie, L. Liu, S. Deng, D. Zhao, Z. Niu, *Angew. Chem. Int. Ed.* **2020**, *59*, 4920.
- [16] Q. Zhao, W. Huang, Z. Luo, L. Liu, Y. Lu, Y. Li, L. Li, J. Hu, H. Ma, J. Chen, *Sci. Adv.* **2018**, *4*, eaao1761.
- [17] H. Glatz, E. Lizundia, F. Pacifico, D. Kundu, *ACS Appl. Energ. Mater.* **2019**, *2*, 1288.
- [18] C. Zhong, B. Liu, J. Ding, X. Liu, Y. Zhong, Y. Li, C. Sun, X. Han, Y. Deng, N. Zhao, W. Hu, *Nat. Energy* **2020**, *5*, 440.
- [19] Y. Liu, L. Xie, W. Zhang, Z. Dai, W. Wei, S. Luo, X. Chen, W. Chen, F. Rao, L. Wang, Y. Huang, *ACS Appl. Mater. Interfaces* **2019**, *11*, 30943.
- [20] S. Zuo, X. Xu, S. Ji, Z. Wang, Z. Liu, J. Liu, *Chem. A Eur. J.* **2021**, *27*, 830.
- [21] Z. Luo, S. Zheng, S. Zhao, X. Jiao, Z. Gong, F. Cai, Y. Duan, F. Li, Z. Yuan, *J. Mater. Chem. A* **2021**, *9*, 6131.
- [22] G. Dawut, Y. Lu, L. Miao, J. Chen, *Inorg. Chem. Front.* **2018**, *5*, 1391.
- [23] Z. Guo, Y. Ma, X. Dong, J. Huang, Y. Wang, Y. Xia, *Angew. Chem.* **2018**, *57*, 11737.
- [24] K. Zhou, H. Yan, Q. Tang, Z. Luo, X. Wang, F. Cai, *J. Power Sources* **2024**, *591*, 233854.
- [25] Y. Zhang, L. Zhao, Y. Liang, X. Wang, Y. Yao, *eScience* **2022**, *2*, 110.

- [26] C. Song, Q. Wang, R. Wen, Q. Tang, Z. Luo, Z. Yuan, *Small Methods* **2024**, *8*, 202300809.
- [27] B. Niu, J. Wang, Y. Guo, Z. Li, C. Yuan, A. Ju, X. Wang, *Adv. Energy Mater.* **2024**, *14*, 2303967.
- [28] T. Sun, J. Pan, W. Zhang, X. Jiang, M. Cheng, Z. Zha, H. J. Fan, Z. Tao, *Nano-Micro Lett.* **2024**, *16*, 46.
- [29] Y. Shi, P. Wang, H. Gao, W. Jin, Y. Chen, Y. Huang, T. R. Wu, D. Y. Wu, J. Xu, J. Cao, *Chem. Eng. J.* **2023**, *461*, 141850.
- [30] Y. Liang, Y. Jing, S. Gheytani, K. Y. K.-Y. Lee, P. Liu, A. Facchetti, Y. Yao, *Nat. Mater.* **2017**, *16*, 841.
- [31] A. Yu, Q. Pan, M. Zhang, D. Xie, Y. Tang, *Adv. Funct. Mater.* **2020**, *30*, 2001440.
- [32] M. E. Speer, M. Kolek, J. J. Jassoy, J. Heine, M. Winter, P. M. Bieker, B. Esser, *Chem. Commun.* **2015**, *51*, 15261.
- [33] Y. Song, Q. Qin, L. Jing, M. Li, H. Zhao, J. Cui, Y. Zhang, *Composites Part B* **2023**, *252*, 110517.
- [34] W. Yang, X. Du, J. Zhao, Z. Chen, J. Li, J. Xie, Y. Zhang, Z. Cui, Q. Kong, Z. Zhao, C. Wang, Q. Zhang, G. Cui, *Joule* **2020**, *4*, 1557.
- [35] C. Wang, Q. Ji, R. Chu, Z. Ullah, M. Zheng, X. Dong, Y. Sun, Q. Li, L. Liu, *ACS Appl. Energ. Mater.* **2021**, *4*, 12641.
- [36] H. Yang, Y. Wang, P. Wang, X. Liu, Y. Liang, W. Ni, G. Xu, X. Wei, L. Yang, *Chem. Eng. J.* **2023**, *457*, 141140.
- [37] N. Al-Ansi, A. Salah, Z.-Y. Gu, Q. A. Drmosh, G.-D. Yang, J.-Y. Zhang, M. Sajid, X.-L. Wu, J.-P. Zhang, L. Zhao, H.-Z. Sun, *ACS Appl. Nano Mater.* **2023**, *6*, 19876.
- [38] W. Li, H. Xu, H. Zhang, F. Wei, L. Huang, S. Ke, J. Fu, C. Jing, J. Cheng, S. Liu, *Nat. Commun.* **2023**, *14*, 5235.
- [39] Z. Chen, H. Cui, Y. Hou, X. Wang, X. Jin, A. Chen, Q. Yang, D. Wang, Z. Huang, C. Zhi, *Chem* **2022**, *8*, 2204.
- [40] T. Sun, W. Zhang, Q. Nian, Z. Tao, *Nano-Micro Lett.* **2023**, *15*, 36.
- [41] K. Liu, J. Zheng, G. Zhong, Y. Yang, *J. Mater. Chem.* **2011**, *21*, 4125.
- [42] J. R. Y.-F. W. O. P. Y. C. C. P. Scheffer, *J. Am. Chem. Soc.* **1985**, *107*, 4898.
- [43] A. S. Nabilah Al-Ansi Qasem, A. Drmosh, Guo-Duo Yang, A. Hezam, A. Al-Salihy, J. L. Xing-Long, W. Liang, Z. Jing-Ping, Z. Shao-lei, W. Hai-Zhu Sun, *Small* **2023**, *2023*, 2304459.
- [44] N. Al-Ansi, A. Salah, J. Lin, G. D. Yang, H. Z. Sun, L. Zhao, *Appl. Energy* **2023**, *334*, 120691.
- [45] F. Zheng, Z. Wei, H. Xia, Y. Tu, X. Meng, K. Zhu, J. Zhao, Y. Zhu, J. Zhang, Y. Yang, D. Deng, *J. Energy Chem.* **2022**, *65*, 26.
- [46] A. Salah, H. Da Ren, N. Al-Ansi, H. Tan, F. Yu, L. Yanchun, B. M. Thamer, A. Al-Salihy, L. Zhao, Y. Li, *J. Colloid Interface Sci.* **2023**, *644*, 378.
- [47] P. Wang, J. Tian, J. Hu, X. Zhou, C. Li, *ACS Nano* **2017**, *11*, 7390.
- [48] J. Xiong, J. Li, J. Shi, X. Zhang, W. Cai, Z. Yang, H. Cheng, *Appl. Catal. B* **2019**, *243*, 614.
- [49] S. Mondal, P. Samanta, R. Sahoo, T. Kuila, M. C. Das, *Chem. Eng. J.* **2023**, *470*, 144340.
- [50] Z. Sang, J. Liu, X. Zhang, L. Yin, F. Hou, J. Liang, *ACS Nano* **2023**, *17*, 3077.
- [51] S. Kong, Y. Feng, Z. Xu, X. Wang, X. Zhang, X. Lan, Z. Ma, Y. Yao, Z. Yong, Q. Li, *Electrochim. Acta* **2023**, *440*, 141762.
- [52] S. Wang, J. Zhang, O. Gharbi, V. Vivier, M. Gao, M. E. Orazem, *Nat. Rev. Methods Prim.* **2021**, *1*, 41.
- [53] Z. Song, Y. Qian, T. Zhang, M. Otani, H. Zhou, *Adv. Sci.* **2015**, *2*, 1500124.
- [54] Y. Shi, J. Yang, J. Yang, Z. Wang, Z. Chen, Y. Xu, *Adv. Funct. Mater.* **2022**, *32*, 2111307.
- [55] H. Yan, X. Zhang, Z. Yang, M. Xia, C. Xu, Y. Liu, H. Yu, L. Zhang, J. Shu, *Coord. Chem. Rev.* **2022**, *452*, 214297.
- [56] T. Sun, W. Zhang, Z. Zha, M. Cheng, D. Li, Z. Tao, *Energy Storage Mater.* **2023**, *59*, 102778.
- [57] U. Ali, B. Liu, H. Jia, Y. Li, Y. Li, Y. Hao, L. Zhang, S. Xing, L. Li, C. Wang, *Small* **2023**, *2023*, 2305866.
- [58] M. Yu, N. Chandrasekhar, R. K. M. Raghupathy, K. H. Ly, H. Zhang, E. Dmitrieva, C. Liang, X. Lu, T. D. Kühne, H. Mirhosseini, I. M. Weidinger, X. Feng, *J. Am. Chem. Soc.* **2020**, *142*, 19570.
- [59] T. Ma, Q. Zhao, J. Wang, Z. Pan, J. Chen, *Angew. Chem. Int. Ed.* **2016**, *55*, 6428.
- [60] J. Li, H. Yao, H. Guan, Z. Sun, X. Ling, S. Guan, *ACS Sustainable Chem. Eng.* **2024**, *12*, 4328.
- [61] Y. Wang, C. Wang, Z. Ni, Y. Gu, B. Wang, Z. Guo, Z. Wang, D. Bin, J. Ma, Y. Wang, *Adv. Mater.* **2020**, *32*, 2000338.

Manuscript received: October 16, 2024  
Revised manuscript received: December 10, 2024  
Accepted manuscript online: December 10, 2024  
Version of record online: January 3, 2025